



High Rank Coal Pore Fracture Structure and its Impact on Reservoir Characteristics in the Southern Qinshui Basin

Changjiang Ji^{1,2,3*}, Guofu Li^{2,3}, Haijin Hao^{2,3}, Zhimin Song¹ and Dingding Guo^{2,3}

¹Henan Polytechnic University, Jiaozuo, China, ²State Key Laboratory of Coal and CBM Co-mining, Jincheng, China, ³Yi'an-Lanyan Coal and CBM Co-mining Technology CO., LTD, Jincheng, China

Although the southern Qinshui Basin is the most successful area for coalbed methane (CBM) development in China, the production of CBM wells in different blocks in the area is significantly different. One of the key reasons is the difference in pore structure in various-ranked coal. In this study, No. 3 coal seam of Sihe and Zhaozhuang blocks in southern Qinshui Basin was selected as the research object to investigate the high rank coal pore fracture structure and its impact on reservoir characteristics. Mercury intrusion porosimetry (MIP), low-temperature liquid nitrogen adsorption (LTN₂A), scanning electron microscopy (SEM), and isothermal adsorption tests were conducted. The results show that the Sihe No.3 coal seam was mainly composed of open cylindrical and flat pores with a high proportion of transition pores (10–100 nm), large specific surface area, good connectivity, strong adsorption capacity, high gas content, and reservoir energy. Zhaozhuang No.3 coal had high proportion of mesopores (100–1,000 nm), small specific surface area, poor pores connectivity, weak adsorption capacity, poor gas content, low reservoir energy, and critical desorption pressure. The proportion of cylindrical pores, parallel plate pores, and wedge-shaped pores closed at one end was high. The anomalies in pore morphology and pore structure characteristics of coal reservoir were the main factors that caused variation in gas production of No.3 coal seam in Sihe and Zhaozhuang blocks.

Keywords: southern Qinshui Basin, high rank coal, pore structure, pore type, reservoir characteristic

OPEN ACCESS

Edited by:

Yiwen Ju,
University of Chinese Academy of
Sciences, China

Reviewed by:

Yingfeng Sun,
University of Science and Technology
Beijing, China
Jian Shen,
China University of Mining and
Technology, China

*Correspondence:

Changjiang Ji
289218603@qq.com

Specialty section:

This article was submitted to
"Economic Geology",
a section of the journal
Frontiers in Earth Science

Received: 23 December 2021

Accepted: 31 January 2022

Published: 16 March 2022

Citation:

Ji C, Li G, Hao H, Song Z and Guo D
(2022) High Rank Coal Pore Fracture
Structure and its Impact on Reservoir
Characteristics in the Southern
Qinshui Basin.
Front. Earth Sci. 10:842275.
doi: 10.3389/feart.2022.842275

INTRODUCTION

Coalbed methane (CBM) is the typical natural gas stored in the pores of gas reservoirs. The pore-fracture system of coal is not only the storage site for CBM, but also the gas migration channel (Tang et al., 2015; Zhao et al., 2016; Lau et al., 2017). Therefore, the pore-fracture structure of coal has an important impact on the adsorption/desorption capacity of CBM, which directly determines the gas content and development potential of coal reservoir (Li et al., 2017; Mou et al., 2021).

Many test methods are used to study the pore-fracture development characteristics, such as mercury intrusion porosimetry (MIP) (Debelak and Schrodt, 1979; Okolo et al., 2015; Sun et al., 2017; Ju et al., 2018; Gao et al., 2018), low temperature N₂/CO₂ adsorption (LTN₂/CO₂A) (Clarkson and Bustin, 1999; Wang et al., 2020; Yan et al., 2020; Mou et al., 2021; Pan et al., 2019), synchrotron small-angle X-ray scattering (SAXS) (Bale and Schmidt, 1984; Shi et al., 2018), small-angle neutron scattering (SANS) (Mastalerz and Oppel, 2012), low field nuclear magnetic resonance (NMR) (Yao

et al., 2010; Yao and Liu, 2012; Yao et al., 2014), atomic force microscope (AFM) (Pan et al., 2015), micro focus X-ray computed tomography (MFX-CT) (Mazumder et al., 2006), scanning electron microscope (SEM) (Klaver et al., 2012), transmission electron microscopy (TEM) (Song et al., 2019), and field emission-scanning electron microscopy (FE-SEM). Many scholars have studied the pore-fracture structure characteristics of coal and obtained significant achievements. The structural characteristics of mesoporous fractures in high rank coal in Qinshui Basin were analyzed by low field NMR, CT reconstruction analysis, and SEM (Song et al., 2018).

Based on the analysis of the characteristics of pore-fracture in coal, the control mechanism of pore structure on CBM adsorption and desorption were discussed (Zhang et al., 2005; Meng et al., 2015; Ma et al., 2018; Xu et al., 2020). The influence of pores on CBM production was studied and discussed by conducting CBM production tests combined with the pore structure characterization of tectonic coal (Jiang et al., 2016).

The Sihe block and Zhaozhuang block of Jincheng mining area are located in the southeast Qinshui Basin, situated approximately 60 km apart. They have the same geological evolution history, simple structural development, and similar underground hydrogeological conditions (Lu et al., 2012; Shi et al., 2017; Xu et al., 2019). The coal seams of interest are No. 3 of Shanxi formation, and No. 9 and No. 15 of Taiyuan formation. The thickness of No. 3 coal in Sihe block is within the range of 3.4–8.7 m, with an average thickness of 6.2 m. While the thickness in Zhaozhuang block is within the range of 1.1–6.6 m, with an average thickness of 4.7 m., the No. 3 coal seam is anthracite and most of the burial depth is no more than 800 m. There is little difference in multiple geological factors. The CBM development technology and process are similar, but the gas production is significantly different. Taking the vertical well of No. 3 coal as an example, the average production of a single well in Sihe block is more than 1,500 m³/d, while the well in Zhaozhuang block is less than 300 m³/d.

Many factors affect the productivity of CBM wells which could be summarized into three categories: geological conditions (Zhang et al., 2017; Ni et al., 2016), reservoir conditions (Guo et al., 2018; Zhao et al., 2017), and engineering conditions (Jia et al., 2017; Wang et al., 2019). Geological conditions include geological evolution history, structural characteristics, burial depth, and hydrogeological characteristics (Song et al., 2005; Qin et al., 2008; Li et al., 2010; Zhao et al., 2012; Sun et al., 2014; Wang et al., 2014; Ji et al., 2018; Wang et al., 2018). Reservoir conditions include gas content, coal thickness, permeability, and coal mass structure characteristics (Zuo et al., 2011; Kang et al., 2017; Xu et al., 2019). Engineering conditions include drilling, cementing, fracturing, and drainage. Therefore, when the geological and engineering conditions are basically the same, the reservoir conditions may be the direct factor causing the difference in CBM production from the gas wells in the Sihe and Zhaozhuang blocks.

Micro-pores are the main storage sites of CBM and macro fractures are the migration channels. Micro fractures are the bridge between the micro-pores and the macro fractures (Fu et al., 2001). Therefore, the pore-fracture structure is the innate factor

determining the reservoir conditions. In order to reveal the difference of reservoir conditions between Sihe and Zhaozhuang blocks, we used No. 3 coal seam as the research interest. Based on the micro scale development characteristics of pore fracture structure, the deep control mechanism of coal reservoir characteristics is analyzed which will provide guidance for CBM development in the southern Qinshui Basin.

SAMPLES AND EXPERIMENT METHODS

Experimental Samples

The samples used in this study were collected from No.3 coal seam of Sihe (SH) and Zhaozhuang (ZZ) blocks which are located in the southeast Qinshui Basin, China, as shown in **Figure 1**.

Using SDLA618 proximate analyzer and referring to the China National Standards GB/T 212-2008 (Proximate analysis of coal), 100 g of air-dried base coal sample less than 0.2 mm (80 mesh) was used for proximate analysis. At the same time, the maximum vitrinite reflectivity (Ro, max) of samples was measured according to China National Standards GB/T 6948-2008 (Method of determining microscopically the reflectance of vitrinite in coal). The experimental results are listed in **Table 1**.

Experimental Work

Mercury Intrusion Porosimetry

Mercury intrusion porosimetry (MIP) uses external pressure to make mercury overcome surface tension into pores to measure the porosity of porous media. Analysis of mercury intrusion was carried out by Autopore IV 9505, which was an automatic mercury intrusion instrument produced by American Michael Instrument Company. Following China National Standards GB/T 21650.1-2008 (Pore size distribution and porosity of solid materials by mercury porosimetry and gas adsorption—Part 1: Mercury porosimetry), samples with diameter of 2.5 cm and length of 2.2 cm were dried at 110°C for 4 h. The dried and degassed samples were used in the MIP test within the pressure up to 120 MPa.

Low Temperature Nitrogen Adsorption-Desorption

ASAP2020 automatic specific surface area (SSA) and porosity analyzer produced by American Michael Instrument Company was used in the experiment. The pore size analysis is within 0.35–500 nm (nitrogen adsorption). The isothermal adsorption/desorption line is obtained according to the isothermal adsorption principle of “static volumetric method”. Referring to Chinese Petroleum Industry Standard SY/T 6154-1995 (Determination of specific surface and pore size distribution of rocks—Static adsorption capacity method), the coal samples were pulverized to the particle size of 0.28–0.45 mm (40–60 mesh), where each sub-sample was 5–10 g. Before the test, samples were treated for 8 h at the temperature of 105°C to remove residual gases and moisture. The adsorption experiment was conducted after locating the samples into the analyzer and setting the testing pressure. SSA, pore diameter, and pore volume (PV) were automatically calculated through pre-selected models, including Brunauer–Emmett–Teller (BET) and Barret-Joyner-

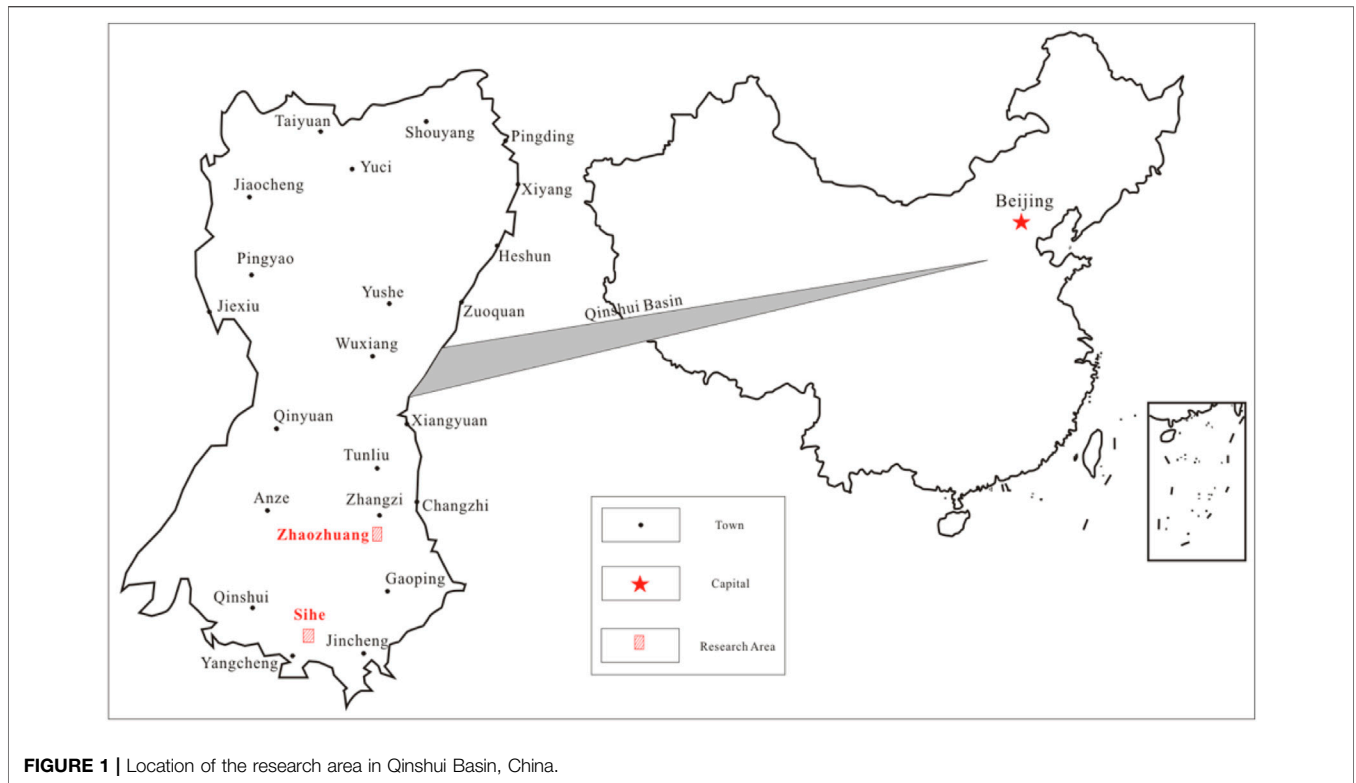


FIGURE 1 | Location of the research area in Qinshui Basin, China.

TABLE 1 | No.3 coal industry analysis results.

Locations	Mad (%)	Ad (%)	Vdaf (%)	FCad (%)	Ro, max (%)
SH	2.08	9.10	5.83	83.00	3.31
	2.41	8.68	7.36	81.63	3.51
ZZ	1.36	8.16	10.26	80.28	2.74
	1.02	9.28	9.86	79.85	2.65

Note: Mad = moisture; Ad = ash; Vdaf = volatile matter; FCad = fixed carbon; Ro,max = Maximum vitrinite reflectivity.

Halenda (BJH) (Brunauer et al., 1938; Li X et al., 2018; Zhang et al., 2021).

Scanning Electron Microscope

Using an EVO MA15 SEM produced by Carl Zeiss of Germany, 3 nm, 4 nm, 10 nm, and 20 nm microscopic image observation can be achieved under SE high vacuum mode, BSE variable pressure mode, 3 kV high vacuum mode, and 1 kV high vacuum mode, respectively. The magnification ranges from 5-1000000 times. The maximum sample height is 145 mm and the maximum sample diameter is 250 mm. Referring to Chinese Petroleum Industry Standard SY/T 5162-2014 (Analytical method of rock sample by SEM), and the pore-fracture characteristics were observed under SEM. The sub-samples with the size smaller than 1 cm × 1 cm × 1 cm were considered appropriate for testing. After polishing a smooth and flat surface, samples were fixed on the sample holders and sprayed with conductive film. Then, the samples were placed on

the SEM stage and pore -fractures were observed under different magnifications.

Isotherm Adsorption Experiment

Following the China National Standards GB/T 474-2008 (Method for preparation of coal sample), the sub-samples were pulverized to the particle size between 60 and 80 mesh to perform methane adsorption isotherm experiments by using the Isotherm Adsorption/Desorption System ISO-300 (TerraTek Company, Inc., Utah, USA). The system working pressure and temperature could reach as high as 34.5 MPa and 100°C, respectively. For each sample, according to the China National Standards GB/T 19560-2008 (Experimental method of high-pressure isothermal adsorption to coal), 200 g of pulverized samples were prepared. Then, the samples were placed into the sample cell. The air-dried basis and dry ash-free basis of the samples were carried out. Isothermal adsorption characteristics of No. 3 coal in SH and ZZ blocks were tested under the same range of temperature and pressure. The experimental temperature was 20°C and the pressure range was 0–9 MPa.

RESULTS AND ANALYSIS

Mercury Intrusion Porosimetry Test Results

Two coal samples from the SH and ZZ blocks were selected for the MIP test. Before the test, porosity, permeability, and other parameters of the samples were measured. The basic sample parameters are listed

TABLE 2 | Basic parameters of No.3 coal sample.

sample	length (cm)	diameter (cm)	porosity (%)	horizontal permeability (md)
SH-01	2.287	2.470	3.9	0.0307
SH-02	2.159	2.469	6.5	0.2690
ZZ-01	2.236	2.466	3.6	0.0220
ZZ-02	2.165	2.468	3.3	0.0235

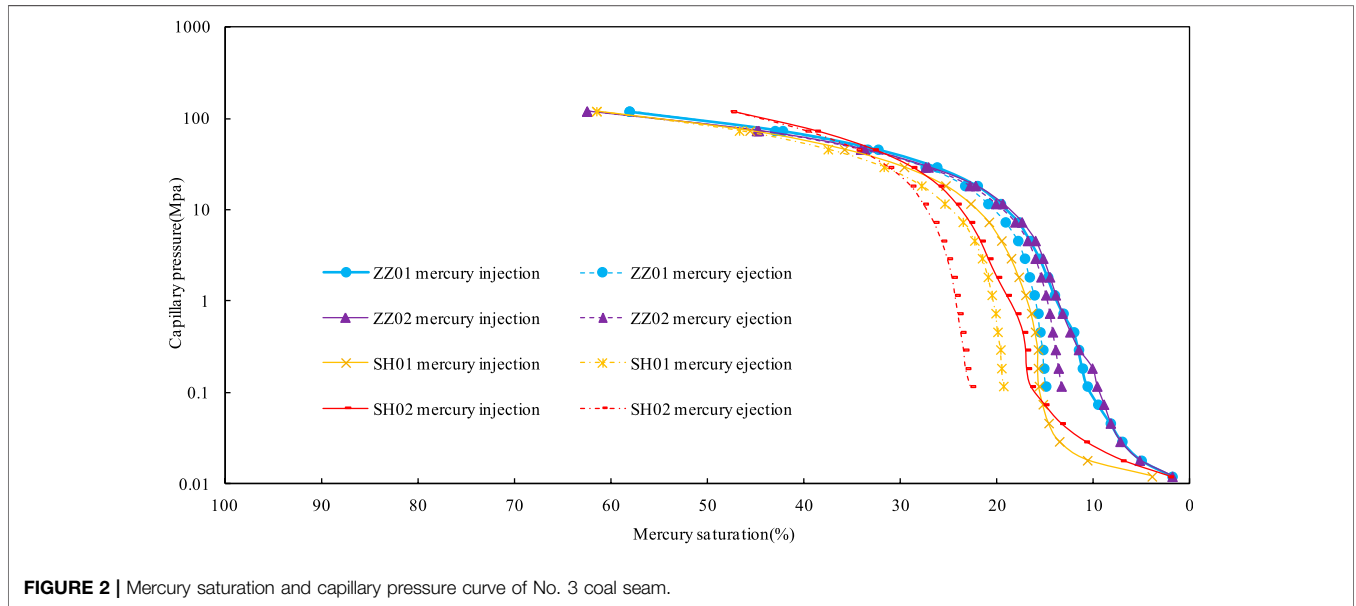


FIGURE 2 | Mercury saturation and capillary pressure curve of No. 3 coal seam.

in **Table 2**. The porosity and horizontal permeability from SH are higher than those from ZZ.

The results of the MIP experiment are presented in **Figure 2**. The total mercury intake in the SH and ZZ blocks is not high, which reflects that micro/transition pores have developed in the blocks (Li CH et al., 2018). However, there are also obvious differences in mercury injection and ejection curves in the blocks.

The total mercury injection in SH is less than that in ZZ. Mercury injection and ejection curves in ZZ almost coincide when the pressure exceeds 10 MPa, while the curves in SH almost coincide until the pressure exceeds 30 MPa. The proportion of micro/transition pores in S is higher.

The hysteresis loop between advance and retreat mercury curves in SH is generally wide, and the hysteresis loop in ZZ is narrow. The large area of the hysteresis loop indicates that the samples are mainly dominated by the open pores with good connectivity. While the hysteresis loop is narrow, there are more semi-closed pores in the sample, and the connectivity of pores is poor, which are not relatively conducive to gas desorption, diffusion, and migration. For lower pressures, the mercury injection rate in SH samples is significantly greater than that in the ZZ samples, which further proves that the pore connectivity in SH sample is good.

Currently, two recommendation methods are often used to characterize pore size classification. One is provided by IUPAC, based on which the pore size distribution is characterized by micropores with the pore size less than 2 nm, mesopores with the pore size between 2 and 50 nm, and macropores with the pore size

greater than 50 nm (International Union of Pure and Applied Chemistry, 1972). The other widely used classification is provided by Hodot in 1966, pore sizes are classified into micropores (<10 nm), transition pores (10–100 nm), mesopores (100–1,000 nm), and macropores (>1,000 nm) (Hodot, 1966). Based on the MIP data, the pore throat radius types and distribution characteristics of samples in two blocks are further analyzed, as presented in **Figure 3**.

According to the Hodot classification scheme, micropores are gas adsorption sites, transition pores are gas diffusion space, mesopores constitute the space for slow gas seepage, and macropores are a strong gas seepage space. Micropores and transition pores are the main spaces for CBM adsorption and diffusion, while mesopores and macropores are the main channels for CBM seepage and migration.

It can be further concluded from **Figure 3** that the largest proportion of pores in SH and ZZ are transition pores, followed by micropores and macropores. However, the proportion of transition pores in the SH sample is high, while the proportion of macropores in ZZ sample is relatively higher. Due to the poor pore connectivity of the ZZ samples, the original porosity and permeability in the ZZ sample are presented in **Table 2** are generally lower than those in SH.

Low Temperature Nitrogen Adsorption-Desorption Test Results

MIP uses external force to inject mercury into pores to measure porosity. Therefore, MIP is more accurate for the measurement of

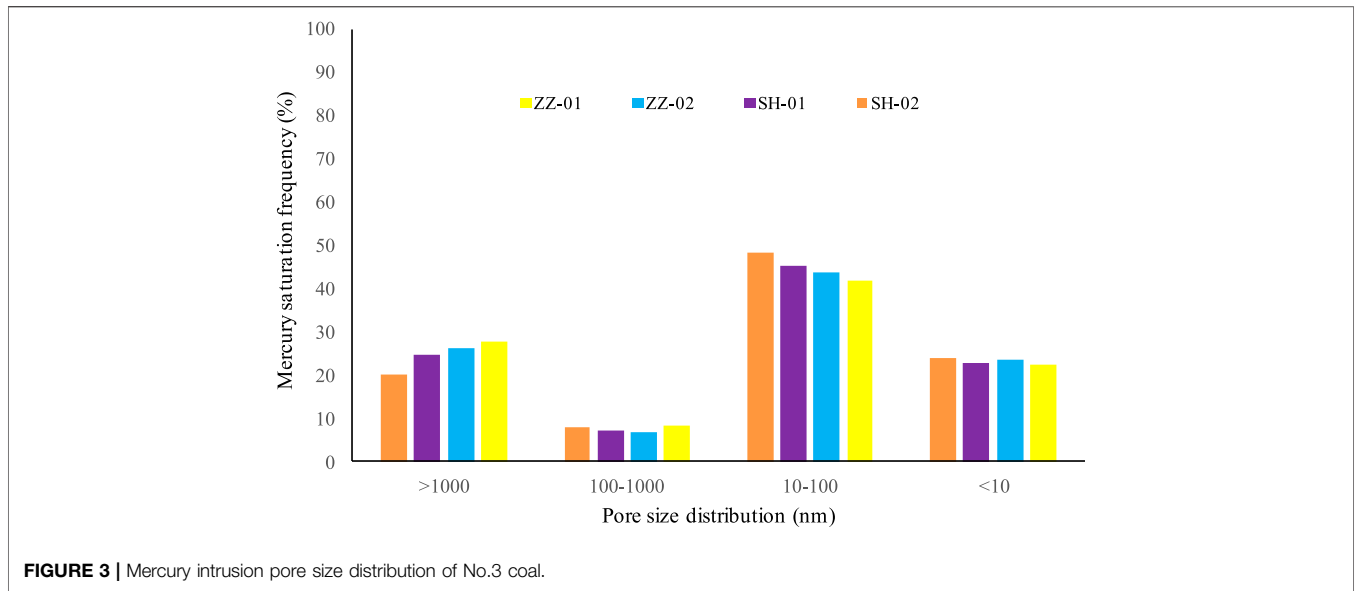


FIGURE 3 | Mercury intrusion pore size distribution of No.3 coal.

TABLE 3 | Porosity test results of No.3 coal seam.

samples	SSA (m ² /g)	PV (cm ³ /g)	Average Pore diameter (nm)	PV (cm ³ /g)			SSA (/m ² /g)		
				<10 nm	10–100 nm	>100 nm	<10 nm	10–100 nm	>100 nm
SH-01	4.0226	0.002866	18.6358	0.000224	0.001793	0.000851	0.361	0.234	0.022
SH-02	6.3530	0.003745	12.7819	0.000750	0.002204	0.000790	0.833	0.319	0.021
ZZ-01	0.3034	0.000623	16.6472	0.000093	0.000293	0.000238	0.104	0.042	0.006
ZZ-02	0.9653	0.003021	23.1727	0.000291	0.001591	0.001140	0.286	0.209	0.028

Note: SSA = Specific surface area (BET); PV = pore volume (BJH).

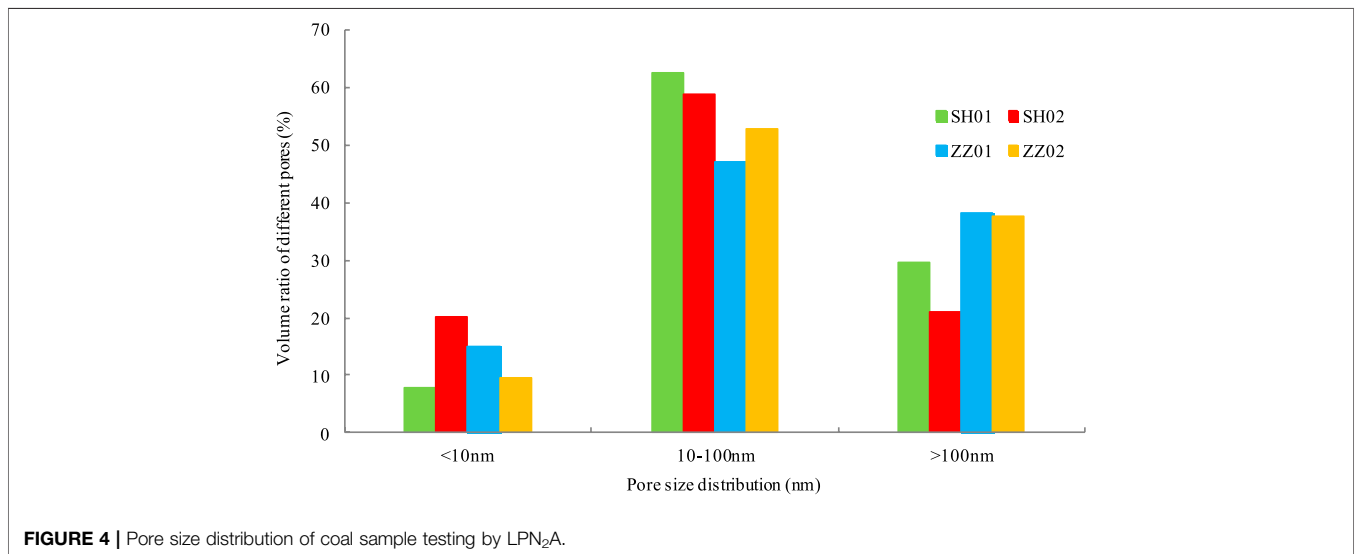


FIGURE 4 | Pore size distribution of coal sample testing by LPN₂A.

macropores and the accuracy becomes less reliable for the measurement of nanopores. The nanopores are inaccessible by mercury, where mercury is only accessible for the pores with the size larger than 3 nm (Clarkson C.R.,2013). Under higher pressures,

many pores will deform or collapse, resulting in deviation from the theoretical values and errors happen in the test results.

The LTN₂A test has a relatively higher reliability in the measurement of nanopores. Therefore, it is necessary to

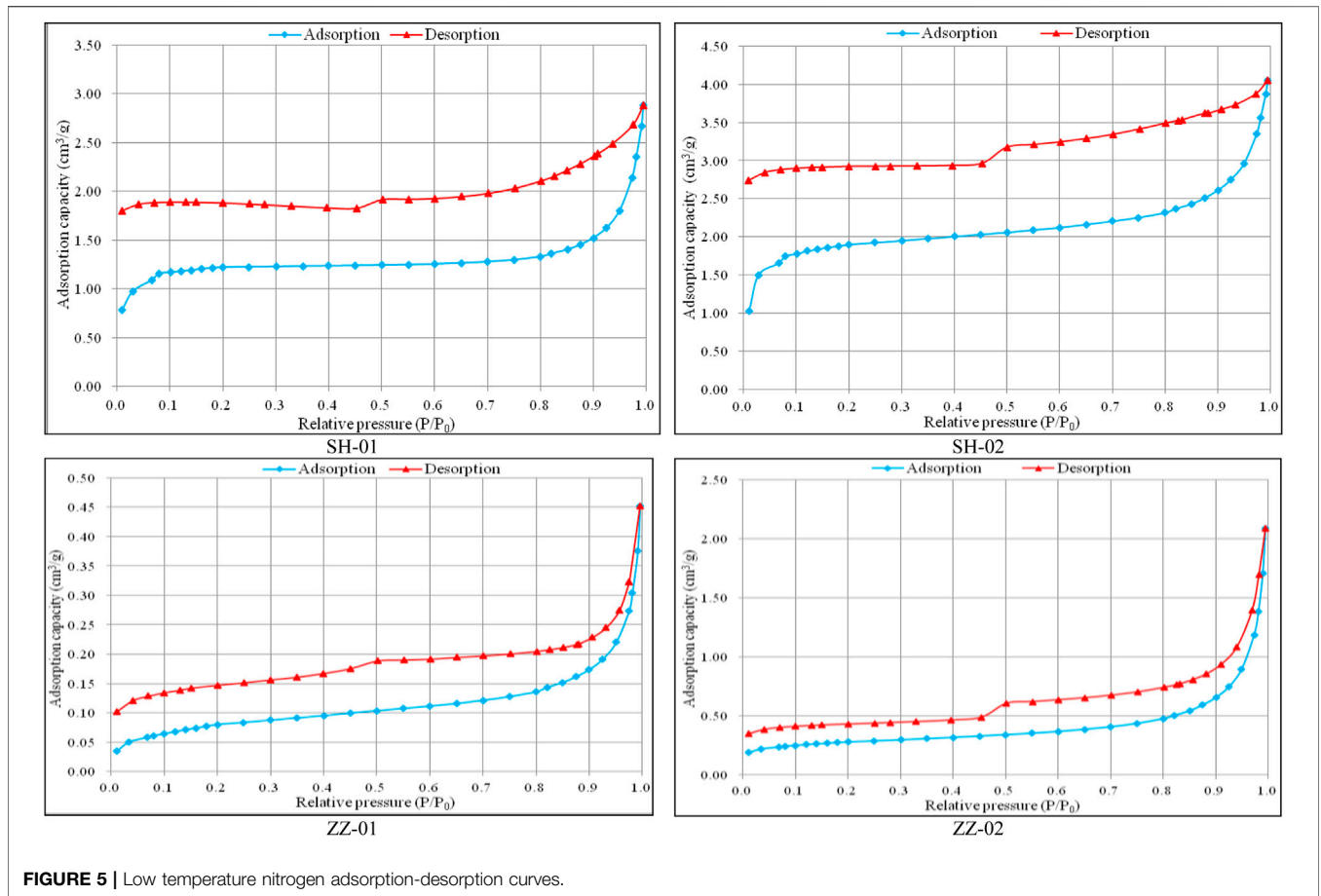


FIGURE 5 | Low temperature nitrogen adsorption-desorption curves.

comprehensively obtain the pore structure characteristics with the combination of the LTN₂A method.

Pore Distribution Characteristics

According to the Hodot classification scheme, the pore distribution characteristics in the SH and ZZ blocks tested by the LTN₂A method are listed in Table 3. The results show that the SSA (BET) in SH coal is obviously larger than that in ZZ. The pore size distribution characteristics of the two blocks are presented in Figure 4.

Pore diameter in SH is ‘centralized’ distribution, where most of them are transition pores (10–100 nm), accounting for about 60%, and the number of mesopores and micropores are relatively smaller. The pore diameter in the ZZ coal is dominated by transition pores and the mesopores are larger than 100 nm. The sum of the two accounts for more than 80%, while the proportion of micropores is less. Therefore, larger pore size is the main reason that the SSA in ZZ is much smaller than that in SH.

Pore Type Analysis

Based on the adsorption and coagulation theory, the separation of adsorption and desorption curves often occurs in the LTN₂A, thus forming the adsorption loop. The size and morphology of the coal pores are different, resulting in great differences in the shape of LTN₂A curves. Therefore, the shape of LTN₂ adsorption

loop could reflect certain pore structure characteristics (Li et al., 2003; Song et al., 2013; Zou et al., 2013). According to previous research results on adsorption-desorption curves (Yan and Zhang, 1979; Chen and Tang, 2001; Yao et al., 2006), combined with de Boer’s classification method of hysteresis loop shape (Boer J et al., 1964), the pore types are mainly classified into five categories (Chen and Tang, 2001): 1) cylindrical pores closed at one end, 2) cylindrical pores open at both ends, 3) parallel plate pores and wedge-shaped pores closed at one end, 4) parallel plate pores open at four sides, and 5) narrow-necked bottle pores. The adsorption and desorption curves of the pores from categories 1 and 3 overlap, which will not produce adsorption loops. The desorption curves of the pores from categories 2 and 4 are separated from the adsorption curves to form an adsorption loop. The pores from category 5 produce an adsorption loop, where there is a sharply declining inflection point in the loop. While open pores are conducive to gas desorption and diffusion, closed pores are not.

The LTN₂A experimental results in the SH and ZZ blocks are presented in Figure 5. In the figure, *P* is the nitrogen partial pressure and *P*₀ is the nitrogen saturated vapor pressure at the temperature of liquid nitrogen. There is an obvious hysteresis loop between the adsorption and desorption curve in SH coal sample. In the adsorption process, when the relative pressure is less than 0.1, the adsorption curve increases rapidly with the

pressure increase. This is due to the nitrogen molecules filling in ultra-micropores and the monolayer adsorption process on the larger pore wall (Lin et al., 2016). Then, the curve rises gently and the adsorption curve does not begin to rise significantly until the relative pressure is greater than 0.9. This indicates that some cylindrical pores with one end closed or parallel-plate pores and wedge-shaped pores with one closed end are distributed. The distance between the adsorption and desorption curves is large, indicating that the pores in SH coal are mainly cylindrical small pores at both ends or parallel plate pores with four sides open. The change in desorption curve is very smooth. At higher relative pressures, the amount of desorbed gas decreases slowly, which means that the diameter of open pores is small. When the relative pressure drops to about 0.5, the desorption curve suddenly falls, which may be caused by the sudden evaporation and release of liquid nitrogen in the “ink bottle” pores. According to Kelvin equation (Eq. 1), the diameter of the “ink bottle” neck is calculated to be less than 3 nm. Therefore, the pore system in SH coal is complex. The pore morphology is mainly categories 2 and 4, and a small amount of categories 1 and 3, where the diameter of the pores is basically small.

$$r = \frac{-2\gamma V_m \cos \varphi}{RT \ln \frac{P}{P_0}} \quad (1)$$

Where, P/P_0 is the relative pressure; γ is the liquid nitrogen surface tension, 8.85×10^{-3} N/m; V_m is the molar volume of liquid nitrogen, 34.65×10^{-4} m³; R denotes the general gas constant, 8.315 J/(K mol); r is the maximum pore radius of capillary condensation, nm; T is the temperature, 77.3 K; and φ denotes the contact angle equal to 0° .

ZZ coal also has an adsorption loop but the distance between the adsorption and desorption curves is close. The two curves almost coincide at a relative higher pressure, indicating that the cylindrical pores, parallel plate pores, or wedge-shaped pores closed at one end, account for a relatively high proportion. The adsorption curve rises steadily for the low pressures, indicating that the diameter of open pores is small. When the relative pressure is higher than 0.8, the adsorption curve increases obviously. When the relative pressure exceeds 0.9, the adsorption capacity increases sharply, and significant capillary condensation occurs, meaning the pore diameter is large. During desorption, as long as the pressure decreases slightly, the desorption capacity increases sharply and the capillary evaporation is obvious. This further indicates the existence of open cylindrical pores and flat pores with larger diameter. Subsequently, as the pressure drops, the desorption capacity also decreases slowly. When the relative pressure drops to 0.5, the desorption capacity suddenly falls, showing that a certain degree of “ink bottle” pores are also developed. Therefore, the pore system in ZZ coal is complex too. Although most of them are still open cylindrical and flat pores with large diameter, the proportion of cylindrical pores, parallel plate pores or wedge-shaped pores closed at one end is also high. A small number of impermeable bottle pores are developed.

Based on the above analysis, although the main pore types in the SH and ZZ coal are open cylindrical and flat pores, the open

pore diameter in ZZ is generally large, and the proportion of cylindrical, parallel plate, or wedge-shaped pore closed at one end is significantly higher than that in SH. This leads to poor pore connectivity, which is not advantageous to the CBM desorption. This is also the main reason why the maximum adsorption volume in SH coal is 2.8–4.1 cm³/g, while that in ZZ coal is only 0.45–2.1 cm³/g. Results are basically consistent with the MIP test conclusion.

Scanning Electron Microscope Observation

In order to further investigate the differences of micro fractures and pores in SH and ZZ coal, samples were cut into 5 mm × 5 mm × 5 mm size by wire cutting machine. Then, EVO MA15 SEM was used to observe the characteristics and connectivity of the pores and micro fissures. The scanning observation results are shown in Figure 6.

Two obvious micro fractures are observed in SH coal, and the fractures are relatively straight with good connectivity between pores and fractures. However, the larger pores with diameter of 1 μm or more were less developed and distributed relatively sparsely. No obvious fractures were observed in the ZZ coal. There are many large pores with a pore diameter greater than 1 μm, but the connectivity between the macropores is poor. The scanning observation results further verified the analytical conclusions of MIP and LTN₂A experiments.

DISCUSSION

Correlations Between Pore Structures and Isothermal Adsorption Characteristics

Isothermal adsorption experiments were carried out on the air-dried and dry ash-free SH and ZZ coal samples. The testing temperature was 20°C and the pressure range was within 0–9 MPa. The experimental results are presented in Figure 7. The methane adsorption amount of coal samples gradually increases with the increase of pressure which follows the Langmuir equation. Equation 2 is used to calculate the critical desorption pressure of the coal seam and the relevant adsorption parameters are listed in Table 4.

$$P_{cd} = \frac{V_A P_L}{V_L - V_A} \quad (2)$$

Where, P_{cd} is the critical desorption pressure, MPa; V_A is the actual gas content, m³/t; P_L is the Langmuir pressure, MPa; and V_L is the Langmuir volume, m³/t.

The results show that the Langmuir volume of SH coal is significantly higher than that of ZZ coal. This indicates that the adsorption capacity of the SH coal is much larger, which is closely related to the large number of transition pores (10–100 nm) and micropores (<10 nm) distributed in SH coal. The smaller the pore, the larger the SSA, and the stronger the adsorption capacity (Ju et al., 2018). The coal seam has higher gas content and larger stored resources. The actual measured data also verify this. The SH No. 3 coal seam has a large amount of CBM resources which provides an energy basis for the long-term high production of CBM wells.

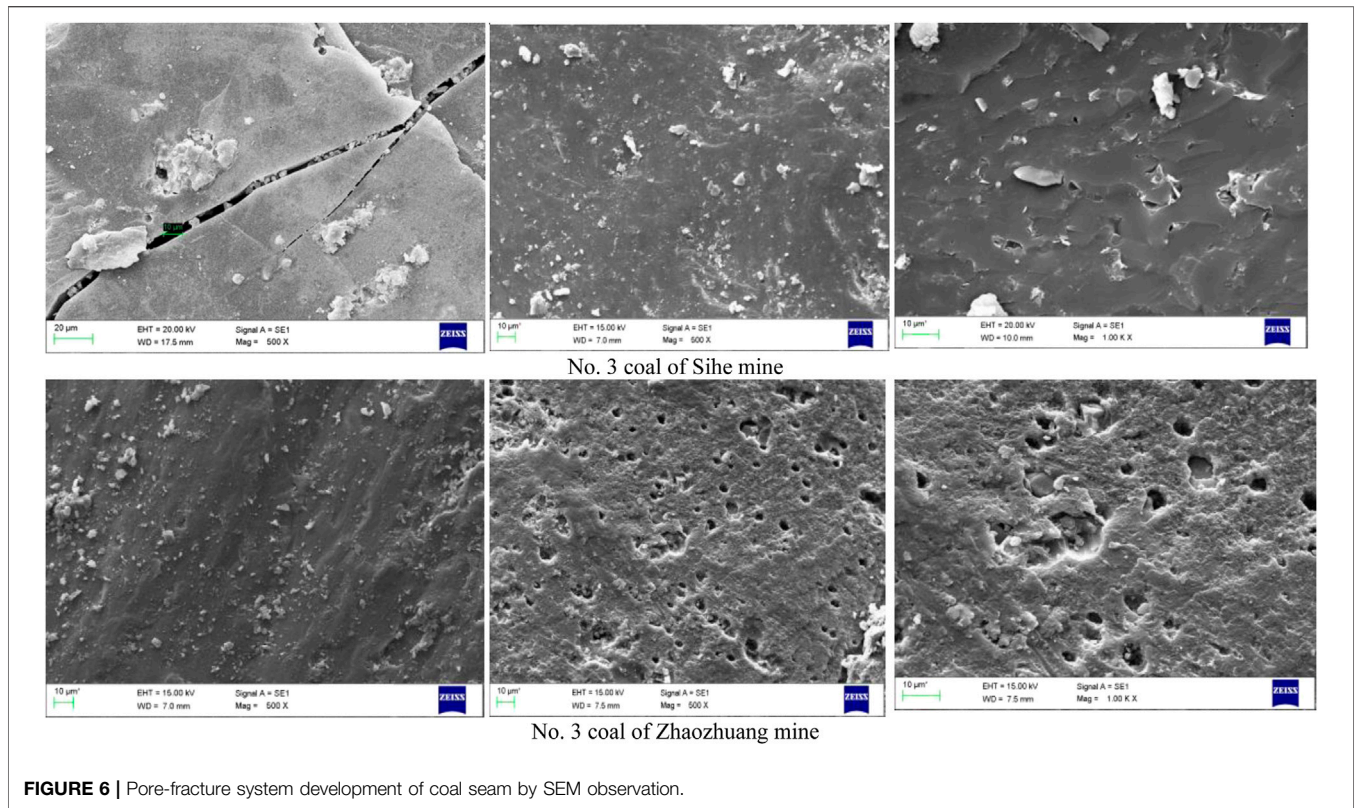


FIGURE 6 | Pore-fracture system development of coal seam by SEM observation.

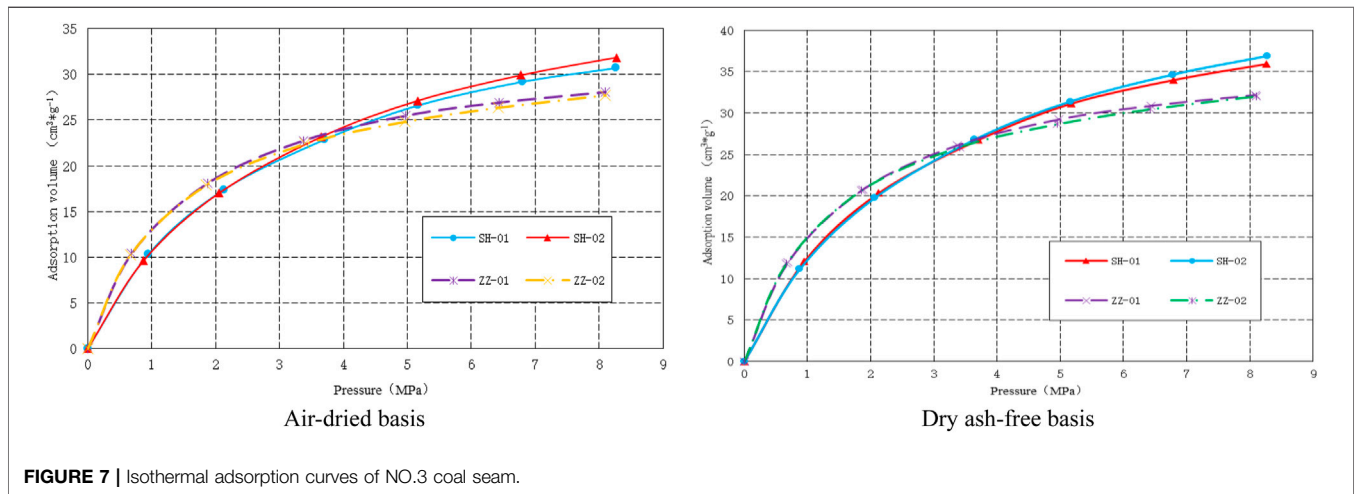


FIGURE 7 | Isothermal adsorption curves of NO.3 coal seam.

The Langmuir pressure of SH coal is also significantly higher than that of ZZ coal. The Langmuir pressure determines the isothermal adsorption curve slope of the low-pressure section and reflects the difficulty of gas adsorbing. The higher the Langmuir pressure, the easier the desorption of adsorbed gas in the coal seam. It takes more time to reach the gas production peak but the production capacity is relatively stable and lasts for a longer time. The smaller the Langmuir pressure, the easier the adsorption. In addition, the desorption efficiency for lower pressures is high. The coal reservoir has higher initial gas production but the continuous gas production time is relatively short.

The slope of isothermal adsorption curves of SH coal for lower pressures is significantly lower than that of ZZ coal, indicating that desorption rate is higher for SH coal. This is related to the pore type and good pore connectivity dominated by cylindrical pores open at both ends, or the parallel plate pores open at four sides. The slope of isothermal adsorption curves of ZZ coal is steep and the desorption of CBM is difficult, mainly because the proportion of cylindrical pores, parallel plate pores, or wedge-shaped pores closed at one end is high, which is not good for the desorption of CBM.

TABLE 4 | Isothermal adsorption parameters of No.3 coal seam.

sample	sample types	V_L (cm^3g^{-1})	P_L (MPa)	V_A (m^3/t)	P_{cd} (MPa)
SH-01	air-dried basis	41.67	2.94	20.90	2.958
	dry ash-free basis	48.71	2.94	24.55	2.987
SH-02	air-dried basis	44.08	3.22	22.40	3.327
	dry ash-free basis	51.08	3.22	25.54	3.220
ZZ-01	air-dried basis	33.40	1.56	15.04	1.278
	dry ash-free basis	38.36	1.56	17.30	1.282
ZZ-02	air-dried basis	32.73	1.53	13.74	1.107
	dry ash-free basis	37.80	1.53	16.33	1.164

Note: V_L = Langmuir volume; P_L = Langmuir pressure; V_A = actual gas content; P_{cd} = critical desorption pressure.

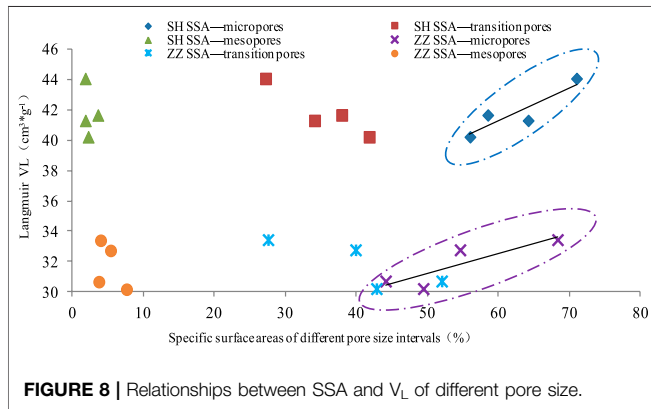


FIGURE 8 | Relationships between SSA and V_L of different pore size.

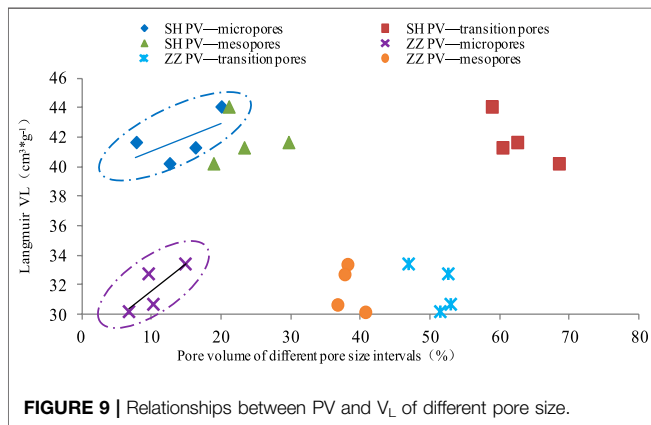


FIGURE 9 | Relationships between PV and V_L of different pore size.

The relationship between the Langmuir volume (V_L), SSA, and PV corresponding to different pore types in coal are shown in **Figures 8, 9**. Micropores in SH and ZZ coal have the most direct impact on V_L . The greater the proportion of micropores in SSA and PV, the higher the V_L . Therefore, the critical desorption pressure of ZZ coal is significantly lower than that of SH coal. In the initial stage of CBM well production, ZZ coal will achieve higher production in shorter time when the bottom-hole pressure drops below the critical desorption pressure, but the life of CBM wells is short. In the early production stage of SH coal, the gas desorbs slowly. However, due to its high critical desorption pressure, CBM wells can achieve long-term high production and life.

Correlations Between Pore Structures and Gas Content Distribution Characteristics

Referring to the China National Standards GB/T 19559-2008 (Method of determining coalbed gas content), through the ground coring test of CBM wells, the gas content in two blocks were obtained by interpolation method, as shown in **Figure 10**.

The results of gas content measurements from CBM wells show that the gas content of SH coal is 8–26 m^3/t , and the gas content in the larger area is concentrated at 16–26 m^3/t . The gas content of ZZ coal is 2–16 m^3/t , and more than half of the area is 6–14 m^3/t . The gas content in most areas of SH No. 3 coal seam is significantly higher than that of ZZ No. 3 coal seam. The main reason is that the proportion of transition pores (10–100 nm) is higher, the SSA is larger, the adsorption capacity of coal is stronger, and the gas content is higher in SH coal pore structure.

Correlations Between Pore Structures and Reservoir Pressure

The results of injection/fall off well test show that the reservoir pressure in both the Sihe and Zhaozhuang blocks is low, usually below 4 MPa, as listed in **Table 5**. The reservoir pressure gradient is also small, which is less than the hydrostatic pressure gradient. Both blocks belong to under-pressure reservoir. The SH reservoir pressure gradient is concentrated within the range of 0.3–0.5 MPa/hm, and the ZZ reservoir pressure gradient is concentrated within the range of 0.2–0.3 MPa/hm, as presented in **Figure 11**. SH No. 3 coal seam has a higher proportion of transition pores (10–100 nm), better connectivity, larger amount of CBM adsorption capacity, and therefore has relatively higher reservoir energy.

In summary, it is the differences in pore types and structural characteristics of coal reservoirs that lead to different adsorption and desorption capacities, resulting in great desorption difficulty in ZZ coal, low critical desorption pressure, small gas content and reservoir pressure gradient, weak reservoir energy, and short duration of gas production. In addition, the connectivity between pores is poor, which makes it difficult for the adsorbed gas far from the wellbore to desorb and migrate to the wellbore, and the life of CBM wells is short. On the contrary, SH coal has less difficulty in gas desorption, larger critical desorption pressure, higher gas content and reservoir pressure

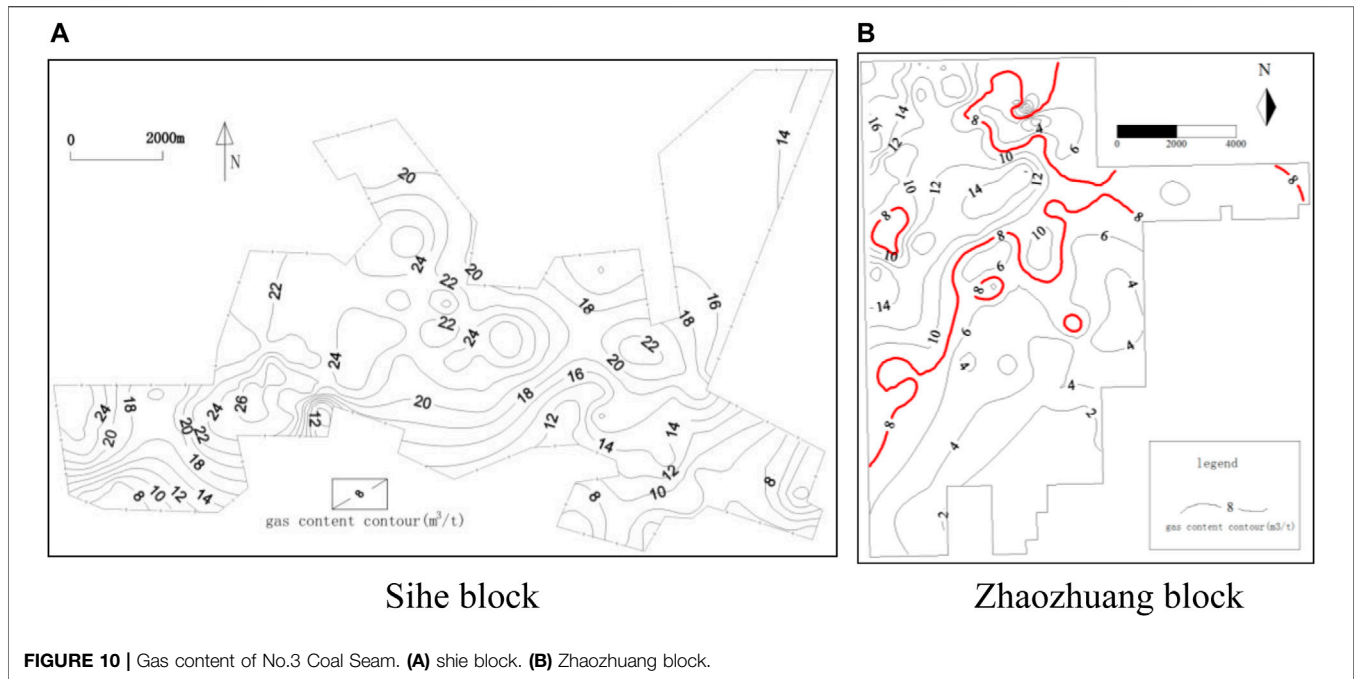


FIGURE 10 | Gas content of No.3 Coal Seam. **(A)** shie block. **(B)** Zhaozhuang block.

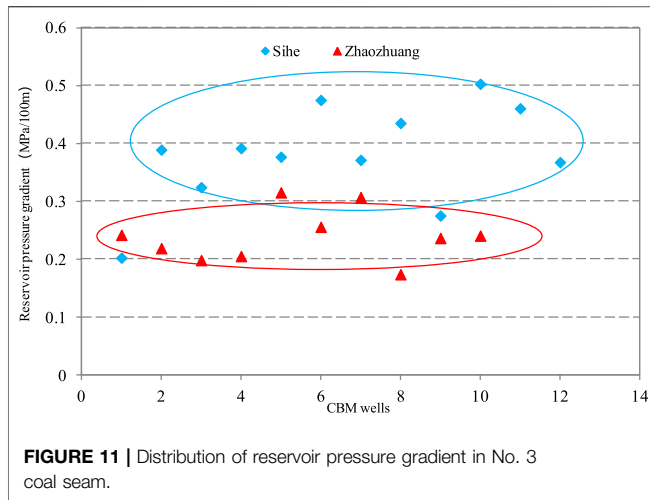
TABLE 5 | Reservoir pressure data of No.3 coal seam.

Block	Well No.	Reservoir pressure /MPa	Depth/m	reservoir pressure gradient/MPa/hm
Shihe	SH001	0.94	463.59	0.203
	SH002	2.56	657.02	0.390
	SH003	2.11	649.80	0.325
	SH004	2.50	637.43	0.392
	SH005	2.47	654.68	0.377
	SH006	3.12	656.16	0.475
	SH007	1.76	473.31	0.372
	SH008	1.61	369.50	0.436
	SH009	1.26	457.12	0.276
	SH010	3.39	673.35	0.503
	SH011	3.53	765.61	0.461
	SH012	1.13	307.09	0.368
Zhaozhuang	ZZ001	2.40	990.61	0.242
	ZZ002	2.10	957.89	0.219
	ZZ003	1.50	755.19	0.199
	ZZ004	1.60	778.18	0.206
	ZZ005	2.40	760.16	0.316
	ZZ006	2.18	851.10	0.256
	ZZ007	2.00	650.41	0.307
	ZZ008	1.30	746.38	0.174
	ZZ009	1.80	760.02	0.237
	ZZ010	1.60	663.95	0.241

gradient, larger reservoir energy, and better pore connectivity. This could contribute to continuous desorption of gas far-field to migrate to the wellbore. Moreover, the high production duration and the life of CBM wells are longer. The wells in the SH block have higher production efficiency.

Regarding the pore structure and morphological characteristics of SH and ZZ coal, some scholars (Gao et al.,

2017) had carried out corresponding research and discussed the difference in reservoir nitrogen adsorption. However, the difference in methane adsorption was not investigated. This study not only analyzed the difference in methane adsorption but also further discussed the impact of pore characteristics on key reservoir parameters, such as gas content and reservoir pressure. In essence, it revealed the underlying reasons for the



significant difference in productivity of CBM wells in the two blocks.

CONCLUSIONS

- 1) SH coal has a high proportion of transition pores (10–100 nm), and the pore morphology is mainly open cylindrical pores and flat pores, with large SSA and good pore connectivity. The transition pores (10–100 nm) and mesopores (100–1,000 nm) are dominant in ZZ coal, with larger pore diameter and smaller SSA. The proportion of cylindrical, parallel plate and wedge-shaped pore closed at one end is high, and the pore connectivity is poor.
- 2) Micropores have a significant impact on the adsorption and desorption capacity of the reservoir. The larger the proportion of micropores, the higher the Langmuir volume (V_L). The V_L and Langmuir pressure (P_L) of SH coal are significantly greater than those of ZZ coal. Moreover, the reservoir has a stronger adsorption energy, lower desorption difficulty, and higher critical desorption pressure.
- 3) The differences in pore types and structural characteristics have a significant impact on coal reservoir characteristics which affect the gas production efficiency of CBM wells. SH coal has more transition pores, stronger adsorption

REFERENCES

- Bale, H. D., and Schmidt, P. W. (1984). Small-Angle X-Ray-Scattering Investigation of Submicroscopic Porosity with Fractal Properties. *Phys. Rev. Lett.* 53 (6), 596–599. doi:10.1103/physrevlett.53.596
- Brunauer, S., Emmett, P. H., and Teller, E. (1938). Adsorption of Gases in Multimolecular Layers. *J. Am. Chem. Soc.* 60 (2), 309–319. doi:10.1021/ja01269a023
- Chen, P., and Tang, X. (2001). The Research on the Adsorption of Nitrogen in Low Temperature and Micro-pore Properties in Coal. *J. China Coal Soc.* 26 (5), 552–556. doi:10.1016/0021-9517(64)90173-3
- Clarkson, C. R., and Bustin, R. M. (1999). The Effect of Pore Structure and Gas Pressure upon the Transport Properties of Coal: a Laboratory and Modeling Study. 2. Adsorption Rate Modeling. *Fuel* 78 (11), 1345–1362. doi:10.1016/s0016-2361(99)00056-3

capacity, higher desorption rate, larger gas content, higher reservoir pressure, stronger formation energy, better pore connectivity, and higher gas production potential. ZZ coal has weaker adsorption capacity, lower formation energy, lower desorption rate, poorer pore connectivity, lower desorption rate in a large area, and poorer gas production capacity of CBM wells.

- 4) In the future for CBM development, different development technologies and processes should be selected according to the differences in reservoir characteristics in Qinshui Basin. For the reservoir similar to the ZZ block, the large-volume fracturing technology of horizontal well can be selected to connect the original pores and fractures to the maximum extent and increase pressure relief desorption area, so as to obtain ideal productivity. For the reservoir similar to SH block, different development technologies and processes can be flexibly selected according to topographical and geological conditions and investment.

DATA AVAILABILITY STATEMENT

The original contributions presented in the study are included in the article/Supplementary Material, further inquiries can be directed to the corresponding author.

AUTHOR CONTRIBUTIONS

CJ: Conceptualization, Methodology, Formal analysis, Writing-original draft, Writing-review and editing. GL: Methodology, Investigation, Supervision. HH: Methodology, Supervision, ZS: Conceptualization Methodology. DG: Editing and revision.

FUNDING

This work was supported by the National Natural Science Foundation of China (41872169; U1910206), and major science and technology projects in Shanxi Province (20191102001; 20181101013).

- Clarkson, C. R., Solano, N., Bustin, R. M., Bustin, A. M. M., Chalmers, G. R. L., He, L., et al. (2013). Pore Structure Characterization of North American Shale Gas Reservoirs Using USANS/SANS, Gas Adsorption, and Mercury Intrusion. *Fuel* 103, 606–616. doi:10.1016/j.fuel.2012.06.119
- Debelak, K. A., and Schrodt, J. T. (1979). Comparison of Pore Structure in Kentucky Coals by Mercury Penetration and Carbon Dioxide Adsorption. *Fuel* 58 (10), 732–736. doi:10.1016/0016-2361(79)90071-1
- Deboer, J., Heuvel, A., and Linsen, B. G. (1964). Studies on Pore Systems in Catalysts IV. The Two Causes of Reversible Hysteresis. *J. Catal.* 3 (3), 268–273. doi:10.1016/0021-9517(64)90173-3
- Fu, X., Qin, Y., Li, G., Li, T., and Hu, C. (2001). An Analysis on the Principal Control Factor of Coal Reservoir Permeability in central and Southern Qinshui Basin, Shanxi [J]. *J. Geomechanics* 7 (1), 45–52. doi:10.3969/j.issn.1006-6616.2001.01.006

- Gao, D., Li, M., Wang, B., Hu, B., and Liu, J. (2017). Characteristics of Pore Structure and Fractal Dimension of Isometamorphic Anthracite. *Energies* 10 (11), 1881. doi:10.3390/en10111881
- Gao, S., Wang, L., Gao, J., and Zhang, R. (2018). Experimental Study on Pore Structures of Hard Coal with Different Metamorphic Grade Based on Fractal Theory. *Coal Sci. Tech.* 46 (8), 93–100. doi:10.13199/j.cnki.cst.2018.08.015
- Guo, G., Xing, L., Liao, X., and Jiang, R. (2018). Analysis of Main Controlling Geological Factors of Production Based on “Three Qualities” of CBM Reservoir. *Nat. Gas Geosci.* 29 (8), 1198–1204. doi:10.11764/j.issn.1672-1926.2018.06.004
- Hodot, B. B. (1966). *Coal and Gas Outburst (Chinese Translation)*. Beijing: China Industry Press.
- IUPAC (1972). Iupac manual of symbols and terminology. *Pure Appl. Chem.* 31, 578.
- Ji, Ch., Hao, H., Hao, Ch., Chen, Zh., Xin, K., Yang, Ch., et al. (2018). Influence Analysis of Groundwater Characteristics to Coalbed Methane Development in Zhaozhuang Block. *Coal Sci. Tech.* 46 (6), 149–154. doi:10.13199/j.cnki.cst.2018.06.025
- Jia, Z., Liu, Sh., Geng, Y., Zhang, H., and Yu, J. (2017). Study on Well Drilling and Completion Engineering Affected to Production of Coalbed Methane Well in Shizhuang Block. *Coal Sci. Tech.* 45 (12), 182–188. doi:10.13199/j.cnki.cst.2017.12.031
- Jiang, W., Zhang, Q., Jiang, Z., and Han, B. (2016). Effect on CBM Drainage Characteristics of Pore Structure of Tectonic Coal. *Nat. Gas Geosci.* 27 (1), 173–179. doi:10.11764/j.issn.1672-1926.2016.01.0173
- Ju, Y., Sun, Y., Tan, J., Bu, H., Han, K., Li, X., et al. (2018). The Composition, Pore Structure Characterization and Deformation Mechanism of Coal-Bearing Shales from Tectonically Altered Coalfields in Eastern China. *Fuel* 234, 626–642. doi:10.1016/j.fuel.2018.06.116
- Kang, Y., Sun, L., Zhang, B., Gu, J., Ye, J., Jiang, Sh., et al. (2017). The Controlling Factors of Coalbed Reservoir Permeability and CBM Development Strategy in China. *Geol. Rev.* 63 (5), 1401–1418. doi:10.16509/j.georeview.2017.05.019
- Klaver, J., Desbois, G., Urai, J. L., and Littke, R. (2012). BIB-SEM Study of the Pore Space Morphology in Early Mature Posidonia Shale from the Hils Area, Germany. *Int. J. Coal Geology.* 103, 12–25. doi:10.1016/j.coal.2012.06.012
- Lau, H. C., Li, H., and Huang, S. (2017). Challenges and Opportunities of Coalbed Methane Development in China. *Energy Fuels* 31 (5), 4588–4602. doi:10.1021/acs.energyfuels.7b00610.1021/acs.energyfuels.7b00656
- Li, Ch., Wei, Y., Wang, A., and Cao, D. (2018). Low-ranked Coal Reservoir Pore Structure Characterized by Mercury Intrusion—A Case Study of Southern Junggar Basin. *Coal Geology. China* 30 (2), 29–33. doi:10.3969/j.issn.1674-1803.2018.02.06
- Li, H., Ogawa, Y., and Shimada, S. (2003). Mechanism of Methane Flow through Sheared Coals and its Role on Methane Recovery☆. *Fuel* 82 (10), 1271–1279. doi:10.1016/s0016-2361(03)00020-6
- Li, M., Liu, Q., Zhang, J., and Wang, L. (2010). Relationship between Structural Style and CBM Well Productivity: A Case Study of the Jincheng coalfield. *Nat. Gas Industry* 30 (11), 10–13. doi:10.3787/j.issn.1000-0976.2010.11.003
- Li, X., Kang, Y., and Haghghi, M. (2018). Investigation of Pore Size Distributions of Coals with Different Structures by Nuclear Magnetic Resonance (NMR) and Mercury Intrusion Porosimetry (MIP). *Measurement* 116, 122–128. doi:10.1016/j.measurement.2017.10.059
- Li, Y., Meng, Sh., Wu, P., and Niu, X. (2017). Accumulation Mechanisms and Classification of CBM Reservoir Types: A Case Study from the Eastern Margin of the Ordos Basin. *Nat. Gas Industry* 37 (8), 22–30. doi:10.3787/j.issn.1000-0976.2017.08.003
- Lin, Y., Jia, X., and Ma, D. (2016). Study and Application of Coal Pore Features Based on Liquid Nitrogen Adsorption Method. *Coal Sci. Tech.* 44 (3), 135–140. doi:10.13199/j.cnki.cst.2016.03.026
- Lu, X., Huang, W., Tang, X., Ao, W., Zhang, Sh., Liu, S., et al. (2012). Impact of limestone of no.15 Coal Seam Roof on the Coalbed Methane Exploitation. *South. Qinshui Basin. Geosci.* 26 (3), 518–526. doi:10.3969/j.issn.1000-8527.2012.03.011
- Ma, D., Wang, Ch., Yang, F., He, Q., Li, Q., Dai, N., et al. (2018). Mass Transfer Process of Desorption of CBM in Dafosi Coal Reservoir. *J. China Coal Soc.* 43 (S1), 219–228. doi:10.13225/j.cnki.jccs.2017.1291
- Mastalerz, M., and Oppel, I. M. (2012). Rational Construction of an Extrinsic Porous Molecular Crystal with an Extraordinary High Specific Surface Area. *Angew. Chem. Int. Ed.* 51 (21), 5252–5255. doi:10.1002/anie.201201174
- Mazumder, S., Wolf, K.-H. A. A., Elewaut, K., and Ephraim, R. (2006). Application of X-ray Computed Tomography for Analyzing Cleat Spacing and Cleat Aperture in Coal Samples. *Int. J. Coal Geology.* 68 (3-4), 205–222. doi:10.1016/j.coal.2006.02.005
- Meng, Zh., Liu, Sh., Wang, B., Tian, Y., and Wu, J. (2015). Adsorption Capacity and its Pore Structure of Coals with Different Coal Body Structure. *J. China Coal Soc.* 40 (8), 1865–1870. doi:10.13225/j.cnki.jccs.2015.0620
- Mou, P., Pan, J., Niu, Q., Wang, Z., Li, Y., and Song, D. (2021b). Coal Pores: Methods, Types, and Characteristics. *Energy Fuels* 35 (9), 7467–7484. doi:10.1021/acs.energyfuels.1c00344
- Mou, P., Pan, J., Wang, K., Wei, J., Yang, Y., and Wang, X. (2021a). Influences of Hydraulic Fracturing on Microfractures of High-Rank Coal under Different *In-Situ* Stress Conditions. *Fuel* 287, 119566. doi:10.1016/j.fuel.2020.119566
- Ni, X., Yang, Y., Wang, Y., and Ye, J. (2016). Study on Gas Production and Water Production Characteristic of CBM Vertical wells under Multi Period Tectonic Movement of Un-development Fault in central South Qinshui Basin. *J. China Coal Soc.* 41 (4), 921–930. doi:10.13225/j.cnki.jccs.2015.0711
- Okolo, G. N., Everson, R. C., Neomagus, H. W. J. P., Roberts, M. J., and Sakurovs, R. (2015). Comparing the Porosity and Surface Areas of Coal as Measured by Gas Adsorption, Mercury Intrusion and SAXS Techniques. *Fuel* 141, 293–304. doi:10.1016/j.fuel.2014.10.046
- Pan, J., Lv, M., Hou, Q., Han, Y., and Wang, K. (2019). Coal Microcrystalline Structural Changes Related to Methane Adsorption/desorption. *Fuel* 239, 13–23. doi:10.1016/j.fuel.2018.10.155
- Pan, J., Zhu, H., Hou, Q., Wang, H., and Wang, S. (2015). Macromolecular and Pore Structures of Chinese Tectonically Deformed Coal Studied by Atomic Force Microscopy. *Fuel* 139, 94–101. doi:10.1016/j.fuel.2014.08.039
- Qin, Y., Jiang, B., Wang, J., Wu, C., Fu, X., Wei, Ch., et al. (2008). Coupling Control of Tectonic Dynamical Conditions to Coalbed Methane Reservoir Formation in the Qinshui basin, Shanxi, China. *Acta Geologica Sinica* 82 (10), 1355–1362. doi:10.3321/j.issn.0001-5717.2008.10.007
- Shi, W., Tang, Sh., Li, Zh., and Zhang, S. (2017). Hydrogen-oxygen Isotope Characteristics of Produced Water from Coal Reservoir of Shanxi Formation in Qinshui basin. *Coal Geology. Exploration* 45 (2), 65–71. doi:10.3969/j.issn.1001-1986.2017.02.011
- Shi, X., Pan, J., Hou, Q., Jin, Y., Wang, Z., Niu, Q., et al. (2018). Micrometer-scale Fractures in Coal Related to Coal Rank Based on Micro-CT Scanning and Fractal Theory. *Fuel* 212, 162–172. doi:10.1016/j.fuel.2017.09.115
- Song, D., He, K., Ji, X., Li, Y., and Zhao, H. (2018). Fine Characterization of Pores and Fractures in Coal Based on a CT Scan. *Nat. Gas Industry* 38 (3), 41–49. doi:10.3787/j.issn.1000-0976.2018.03.005
- Song, X., Wang, S., Cao, T., and Song, Zh. (2013). The Methane Adsorption Features of Cambrian Shales in the Yangtze Platform. *Acta Geologica Sinica* 87 (7), 1041–1048. doi:10.3969/j.issn.0001-5717.2013.07.013
- Song, Y., Jiang, B., Li, M., Hou, C., and Mathews, J. P. (2020). Macromolecular Transformations for Tectonically-Deformed High Volatile Bituminous via HRTEM and XRD Analyses. *Fuel* 263, 116756. doi:10.1016/j.fuel.2019.116756
- Song, Y., Zhao, M., Liu, Sh., Wang, H., and Chen, Zh. (2005). Influence of Structural Evolution to Coalbed Methane Accumulation. *Sci. Bull.* 50 (Suppl. I), 1–5. doi:10.1007/bf03184076
- Sun, F., Wang, B., Li, M., and Liang, H. (2014). Major Geological Factors Controlling the Enrichment and High Yield of Coalbed Methane in the Southern Qinshui Basin. *Acta Petroli Sinica* 35 (6), 1070–1079. doi:10.7623/syxb201406004
- Sun, M., Yu, B., Hu, Q., Yang, R., Zhang, Y., and Li, B. (2017). Pore Connectivity and Tracer Migration of Typical Shales in south China. *Fuel* 203, 32–46. doi:10.1016/j.fuel.2017.04.086
- Tang, D.-Z., Deng, C.-M., Meng, Y.-J., Li, Z.-P., Xu, H., Tao, S., et al. (2015). Characteristics and Control Mechanisms of Coalbed Permeability Change in Various Gas Production Stages. *Pet. Sci.* 12 (4), 684–691. doi:10.1007/s12182-015-0054-5
- Wang, B., Yao, H., Wang, H., Zhao, Y., Li, M., Hu, Q., et al. (2018). Favorable and Major Geological Controlling Factors for Coalbed Methane Accumulation and High Production in the Chengzhuang Block, Qinshui Basin. *Oil And Gas Geology.* 39 (2), 366–372. doi:10.11743/ogg20180215
- Wang, R., Dong, F., Meng, Zh., and Shuai, Zh. (2014). The Controlling Mechanism of Geological Structures on the Production of Coal Bed Methane wells in Fanzhuang Block. *J. China Univ. Mining Tech.* 43 (6), 1025–1030. doi:10.13247/j.cnki.jcmt.000112
- Wang, X., Pan, J., Wang, K., Ge, T., Wei, J., and Wu, W. (2020). Characterizing the Shape, Size, and Distribution Heterogeneity of Pore-Fractures in High Rank

- Coal Based on X-ray CT Image Analysis and Mercury Intrusion Porosimetry. *Fuel* 282, 118754. doi:10.1016/j.fuel.2020.118754
- Wang, X., Zhang, D., Su, E., Jiang, Z., Wang, C., Chu, Y., et al. (2020)10338). Pore Structure and Diffusion Characteristics of Intact and Tectonic Coals: Implications for Selection of CO₂ Geological Sequestration Site. *J. Nat. Gas Sci. Eng.* 81, 103388. doi:10.1016/j.jngse.2020.103388
- Wang, Zh., Yang, J., Chen, L., and Guo, Zh. (2019). Productivity Prediction of Hypotonic CBM Test Well in Jiaozuo Mining Area under Hydraulic Fracturing. *Coal Geology. Exploration* 47 (3), 70–76. doi:10.3969/j.issn.1001-1986.2019.03.012
- Xu, H., Zhou, W., Zhang, R., Liu, S., and Zhou, Q. (2019). Characterizations of Pore, mineral and Petrographic Properties of marine Shale Using Multiple Techniques and Their Implications on Gas Storage Capability for Sichuan Longmaxi Gas Shale Field in China. *Fuel* 241, 360–371. doi:10.1016/j.fuel.2018.12.035
- Xu, Y., and Zhu, Y. (2020). Pore Structure Characteristics of High Rank Coal and its Effect on CBM Desorption. *Nat. Gas Geosci.* 31 (1), 84–92. doi:10.11764/j.issn.1672-1926.2019.10.006
- Xu, Y., Zhu, Y., and Zhang, P. (2019). The Characteristics of Coalbed Methane Production and its Affecting Factors in Zhaozhuang field Qinshui Basin. *Nat. Gas Geosci.* 30 (1), 119–125. doi:10.11764/j.issn.1672-1926.2018.09.005
- Yan, J., Meng, Z., Zhang, K., Yao, H., and Hao, H. (2020)10704). Pore Distribution Characteristics of Various Rank Coals Matrix and Their Influences on Gas Adsorption. *J. Pet. Sci. Eng.* 189, 107041. doi:10.1016/j.petro.2020.107041
- Yan, J., and Zhang, P. (1979). *Adsorption and Coagulation*. Beijing: Science Press.
- Yao, Y., Liu, D., Che, Y., Tang, D., Tang, S., and Huang, W. (2010). Petrophysical Characterization of Coals by Low-Field Nuclear Magnetic Resonance (NMR). *Fuel* 89 (7), 1371–1380. doi:10.1016/j.coal.2014.06.00110.1016/j.fuel.2009.11.005
- Yao, Y., and Liu, D. (2012). Comparison of Low-Field NMR and Mercury Intrusion Porosimetry in Characterizing Pore Size Distributions of Coals. *Fuel* 95, 152–158. doi:10.1016/j.fuel.2011.12.039
- Yao, Y., Liu, D., Huang, W., Tang, D., and Tang, Sh. (2006). Research on the Pore-Fractures System Properties of Coalbed Methane Reservoirs and Recovery in Huainan and Huaibei Coal-fields. *J. China Coal Soc.* 31 (2), 163–168. doi:10.3321/j.issn:0253-9993.2006.02.007
- Yao, Y., Liu, D., and Xie, S. (2014). Quantitative Characterization of Methane Adsorption on Coal Using a Low-Field NMR Relaxation Method. *Int. J. Coal Geology.* 131, 32–40. doi:10.1016/j.coal.2014.06.001
- Zhang, K., Meng, Z., Liu, S., Hao, H., and Chen, T. (2021). Laboratory Investigation on Pore Characteristics of Coals with Consideration of Various Tectonic Deformations. *J. Nat. Gas Sci. Eng.* 91, 103960. doi:10.1016/j.jngse.2021.103960
- Zhang, X., Sang, Sh., Qin, Y., Zhang, J., and Tang, J. (2005). Isotherm Adsorption of Coal Samples with Different Grain Size. *J. China Univ. Mining Tech.* 34 (4), 427–432. doi:10.3321/j.issn:1000-1964.2005.04.005
- Zhang, X., Zhang, Sh., Sun, Q., Yang, Y., and Yang, Y. (2017). Evaluating the Influence of Geological Structure to CBM Productivity Based on AHP and Fuzzy Mathematics. *J. China Coal Soc.* 42 (9), 2385–2392. doi:10.13225/j.cnki.jccs.2017.0061
- Zhao, S., Zhu, Y., Cao, X., Wang, H., and Zhou, Y. (2012). Control Mechanism and Law of Geological Structure Affected to Production Capacity of Coal Bed Methane Well. *Coal Sci. Tech.* 40 (9), 108–111,116. doi:10.13199/j.cst.2012.09.114.zhaoshl.001
- Zhao, X., Jiang, B., Zhang, Sh., Liu, J., Duan, P., and Xu, Q. (2017). Main Controlling Factors of Productivity and Development Strategy of CBM wells in Block 3 on the Eastern Margin of Ordos Basin. *Acta Petrolei Sinica* 38 (11), 1310–1319. doi:10.7623/syxb201711010
- Zhao, X., Yang, Y., Sun, F., Wang, B., Zuo, Y., Li, M., et al. (2016). Enrichment Mechanism and Exploration and Development Technologies of High Rank Coalbed Methane in South Qinshui Basin, Shanxi Province. *Pet. Exploration Dev.* 43 (2), 303–309. doi:10.11698/PED.2016.02.19
- Zou, C., Zhang, G., Yang, Zh., Tao, Sh., Hou, L., Zhu, R., et al. (2013). Geological Concepts, Characteristics, Resource Potential and Key Techniques of Unconventional Hydrocarbon: On Unconventional Petroleum Geology. *Pet. Exploration Developmen* 40 (4), 385–399,454. doi:10.1016/s1876-3804(13)60053-1
- Zuo, Y., Meng, Q., Ren, Y., Jiao, Sh., and Cui, L. (2011). Controlling Factors of Enrichment and High Deliverability of CBM Gas from High-Rank Coal Beds in the Southern Qinshui Basin. *Nat. Gas Industry* 31 (11), 11–13. doi:10.3787/j.issn.1000-0976.2011.11.003

Conflict of Interest: The authors declare that the research was conducted in the absence of any commercial or financial relationships that could be construed as a potential conflict of interest.

Publisher's Note: All claims expressed in this article are solely those of the authors and do not necessarily represent those of their affiliated organizations, or those of the publisher, the editors, and the reviewers. Any product that may be evaluated in this article, or claim that may be made by its manufacturer, is not guaranteed or endorsed by the publisher.

Copyright © 2022 Ji, Li, Hao, Song and Guo. This is an open-access article distributed under the terms of the Creative Commons Attribution License (CC BY). The use, distribution or reproduction in other forums is permitted, provided the original author(s) and the copyright owner(s) are credited and that the original publication in this journal is cited, in accordance with accepted academic practice. No use, distribution or reproduction is permitted which does not comply with these terms.